energies

MDPI

Article

Hygrothermal Analysis of a Museum Storage Room for Metal Cultural Artifacts: Quantification of Factors Influencing High Humidity

Kazuki Ishikawa [1], Chiemi Iba [1,*], Daisuke Ogura [1], Shuichi Hokoi [2] and Misao Yokoyama [3]

[1] Graduate School of Engineering, Kyoto University, Kyoto 6158540, Japan; ishikawa.kazuki.75w@st.kyoto-u.ac.jp (K.I.); ogurad@archi.kyoto-u.ac.jp (D.O.)
[2] School of Architecture, Southeast University, Nanjing 210096, China; hokoi@maia.eonet.ne.jp
[3] Graduate School of Agriculture, Kyoto University, Kyoto 6068502, Japan; misao@kais.kyoto-u.ac.jp
* Correspondence: iba@archi.kyoto-u.ac.jp; Tel.: +81-75-383-2919

Abstract: Several methods for appropriate control of the hygrothermal environment in museums to prevent the deterioration of cultural artifacts were presented in previous studies. However, few detailed hygrothermal simulation models have been used considering the hygrothermal performance of building components and airflow through gaps. Furthermore, hygrothermal properties of a type of storage facility with buffer spaces prevailing in Japan have not been quantitatively evaluated. The objectives of this study were to develop a detailed numerical model of a museum storage room with buffer spaces exhibiting high humidity during summer and to quantitatively evaluate the potential factors causing it; the inflow of humid outdoor air and indirect cooling caused by the air-conditioning system of a surrounding room. We analyzed the simulated temperature and humidity for various cases in which each influencing factor was suppressed. The humidity was reduced when the exhaust fan for the surrounding rooms was stopped or the windows were made airtight, but it hardly changed when the cooling ducts and the reinforced concrete beams were insulated. Thus, the high humidity in the room was attributed to the inflow of humid outdoor air accelerated by the ventilation of surrounding rooms. Although indirect cooling had a small impact on high humidity, its impact on energy loss could still be significant.

Keywords: hygrothermal simulation model; facility operation methods; airflow network model

Citation: Ishikawa, K.; Iba, C.; Ogura, D.; Hokoi, S.; Yokoyama, M. Hygrothermal Analysis of a Museum Storage Room for Metal Cultural Artifacts: Quantification of Factors Influencing High Humidity. *Energies* **2021**, *14*, 3309. https://doi.org/10.3390/en14113309

Academic Editor: Francesco Nocera

Received: 10 May 2021
Accepted: 1 June 2021
Published: 4 June 2021

1. Introduction

Museums and galleries store and exhibit cultural artifacts such as paintings, old documents, and antique metalware. There are various causes of deterioration of these cultural artifacts, for example, deformations caused by rapid changes in temperature and humidity, chemical reactions such as metal corrosion and paper hydrolysis, and biological damage because of mold and insects. The causes of deterioration differ depending on the type of cultural artifacts; however, several of these causes originate and are accelerated because of inappropriate surrounding air temperature and relative humidity (RH) [1–3].

In locations where cultural artifacts are placed, such as museum storage rooms and exhibition halls, maintaining a suitable environment for the artifacts is essential by suppressing changes in temperature and humidity caused by the outdoor air or by visitors. However, improper hygrothermal building performance, air-conditioning (AC) and ventilation systems, and facility operations can produce an inappropriate environment for the conservation of cultural artifacts. Some museum buildings and rooms have poor thermal insulation and insufficient airtightness, leading to air leakage through gaps in windows or doors [4] or small thermal and/or moisture capacity of the wall materials. Others may use AC systems of insufficient capacity [5] or may lack human and financial resources to manage them. In museums located in historic buildings, architectural renovations and

AC system upgrades for the sake of conservation may not be feasible [6] because of the preservation of their heritage value. Some museum buildings have a structure with spaces between the outer walls and the inner walls (side buffer spaces) and attic and crawl spaces to mitigate the influence of outside air. This type of structure is used most frequently in Japan and has been recommended by national organizations [7]. However, difficulties can be encountered while attempting to control the environment and obtain the prescribed temperature and humidity using an AC and ventilation system [4]. This problem is of great practical importance and must be addressed based on the quantitative evaluation of heat, moisture, and air circulation. The inappropriate operation of facilities can lead to the malfunctioning of AC systems that can cause rapid changes in the temperature or humidity around artifacts [4,8]. The unsuitable setpoint of temperature and RH can lead to condensation on the ducts of AC systems or on the building's envelope surfaces [1,4,6], which can cause problems for the conservation of artifacts as well as lead to energy loss or damage to the building. For the safe conservation of cultural artifacts, it is necessary to understand the current state of their surroundings through temperature and humidity monitoring and analytical studies, and to implement appropriate environmental controls by comprehensively considering the buildings, AC and ventilation systems, and operational methods.

Some research has been conducted on the methods for controlling the hygrothermal environment for artifact conservation. For active control, in addition to studies on the design and operation of air conditioners [9–13], environmental control methods using dehumidifiers [14,15], heaters [16,17], and mechanical ventilation [18,19] have been conducted. Janssen et al. [14] studied a method for controlling the temperature and humidity in a museum storage room in Denmark. The authors suggested that the dehumidification load and daily fluctuation of humidity were reduced by improving the airtightness of the storage room and by using moisture buffering of building components. An RH control system operating the dehumidifier at regular intervals was later investigated in a field study [15]. Neuhaus et al. [16] demonstrated the applicability of heating to control RH through a field test and an analytical model of a museum located inside a historical building in the Netherlands. Ferdyn-Grygierek et al. [18] studied a method for controlling the RH in the exhibition space of a museum using a numerical model of a museum, including ventilation and AC. They showed that the combined application of ventilation and temperature control could adjust the RH of the exhibition space to a value suitable for the conservation of the stored materials. In addition, the effectiveness for cultural artifact conservation and energy efficiency of each method were compared [20–23].

Furthermore, several studies have examined the conditions under which passive control of the environment for artifact conservation is possible [24–26]. Padfield et al. [24] and Ryhl-Svendsen et al. [25] showed that the contributions of building thermal inertia, moisture buffering of inner materials, and airtightness are significant for achieving the hygrothermal environment required for the collection conservation based on field surveys in Europe and numerical models.

Thus, the effectiveness of temperature and humidity control methods with and without AC or ventilation systems has been suggested for controlling the hygrothermal environment for cultural artifact conservation. However, few studies have used detailed numerical models of storage environments while considering heat and moisture capacities of buildings and airflow through gaps in building components by simulating heat and moisture transfer in building materials and the amount of air passing through gaps in building components. In addition, the thermal and humidity properties in the storage spaces surrounded by buffer spaces, widely used in Japan, have not been quantitatively evaluated.

The authors conducted a field survey on the temperature and humidity conditions in several storage rooms with a structure with buffer spaces [4] in a museum built in 1986 in Kyoto, Japan, where the climate is characterized by high temperature and humidity in summer (average temperature and RH from July to September of approximately 27 °C and 70%, respectively). A high RH was found during the survey in a storage room for metal cultural artifacts. The International Council of Museums and the International Centre for

the Study of the Preservation and Restoration of Cultural Property have suggested an environment with an RH lower than 45% for the preservation of metallic materials [27]. However, the RH in the room was higher than 45% throughout the year; in summer, specifically, it was higher than 70% [4]. The possible reasons for such a situation were examined on-site and will be summarized in the following section.

A further understanding of the hygrothermal environment in the storage room is necessary to propose proper environmental control methods to ensure a low-humidity environment for the conservation of metal cultural artifacts. In this paper, we developed a hygrothermal simulation model of the storage room with buffer spaces, and we quantitatively evaluated factors that can lead to the high RH in the storage room using the developed numerical model. The numerical model was created by adopting a one-dimensional simultaneous heat and moisture transfer model and a ventilation network model. The heat and moisture balance in the room was calculated by considering the heat and moisture capacities of the building materials and the airflow through gaps in the components.

2. Summary of the Field Survey

From the field survey, some factors to which the high humidity in the storage room could be attributed were determined. There were lavatories on the west side of each floor of the building, and an exhaust fan for them operated constantly (Figure 1). There was, therefore, negative pressure in the corridor leading to the lavatories, which can cause the outdoor air to be drawn into the storage room through the gaps in closed windows. Therefore, the humidity in the storage room might have been more strongly influenced by the humidity of the outdoor air. Another plausible factor was the indirect cooling by an air duct that passed through the attic space of the storage room, as shown in Figure 2. The air duct was used for the return air of the AC system of the upper room, which operated throughout the year at the set temperature and RH of 21 °C and 49%, respectively. The duct was wrapped with 40 mm glass wool and aluminum foil. During the survey, it was found that condensation likely occurred on the duct surface during the cooling period (Figure 3a,b). This could lead to a decrease in the insulation performance of the glass wool. Furthermore, as shown in Figure 2, the upper concrete beam of the attic space was uninsulated and could act as a thermal bridge, resulting in a lower temperature in the storage room owing to the indirect cooling in summer.

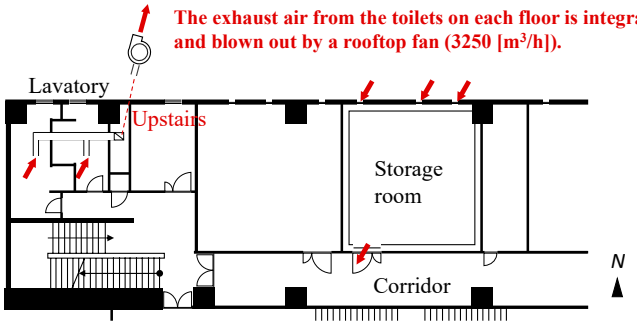

Figure 1. Floor plan around the storage room.

The measurements of temperature and relative humidity were carried out in the room, the attic space, and the northern buffer space since February 2018. The temperature and humidity measured at a point 1.2 m above the floor in the center of the storage room were used for the verification of the numerical model described in Section 3. The logger used for the measurement was the Onset UX100-011 with the specifications shown in Table 1 [28].

Figure 2. The duct passing through the attic space.

(**a**) (**b**)

Figure 3. Traces of condensation on the duct surface: (**a**) gaps in the aluminum foil wrapped around the duct, through which water vapor may enter; (**b**) water stains on the ceiling caused by condensed water falling from the duct.

Table 1. Specification of the Onset UX100-011.

	Temperature	**RH**
Range	−20 °C–70 °C	1–95%RH
Accuracy	±0.21 °C (0–50 °C)	±2.5%RH (10–90%RH)
Resolution	0.024 °C (at 25 °C)	0.01%RH (at 25 °C)
Response time	4 min in air moving 1 m/s	10 s to 90% RH in airflow of 1 m/s

3. Methods

A numerical model was developed uniquely by the authors to simulate the temperature and humidity changes in the storage room. To serve the purpose of this study, the model accounted for the heat and moisture capacity of the building components and the airflow between spaces surrounding the room. Different from other existing models, the influence of the operation of the lavatory fan and heat flow from or into the air conditioning ducts passing through the attic space and the uninsulated beam could be considered to quantitatively evaluate the factor of high humidity in the room.

3.1. Outline of the Storage Room

The target storage room was located on the middle floor of the building, with the northern side facing the outdoor air and the southern side facing the indoor corridor, as shown in Figure 4a,b. The floor area and room volume were approximately 37.8 m^2 and 90.6 m^3, respectively. The thickness of the side buffer space was around 0.2 m; the height of the attic space and the crawl space were 2.4 m and 0.12 m, respectively. The buffer spaces, attic space, and crawl space were connected, allowing air to move between them. The west room and the lower-floor room were non-air-conditioned storage rooms, and the east room was a machine room. The upper-floor room was a storage room that was constantly air-conditioned, as mentioned earlier.

The building was a reinforced concrete (RC) structure, and the outer wall was internally insulated with 50 mm thick extruded polystyrene (XPS) foam. The inner ceiling and walls were supported from the buffer space side with wooden frames. The floor was made of wood, with aluminum foil to provide a vapor barrier and glass wool for thermal insulation. An additional insulation layer (50 mm of XPS) was placed on the inner wall on the north side and covered with gypsum boards. Originally, there were three small windows on both the internal and external walls for ventilation; however, the windows on the inner side were closed to improve the airtightness of the room, and the upper part of the north buffer space was filled with glass wool as airflow stopper, as shown in Figure 4b.

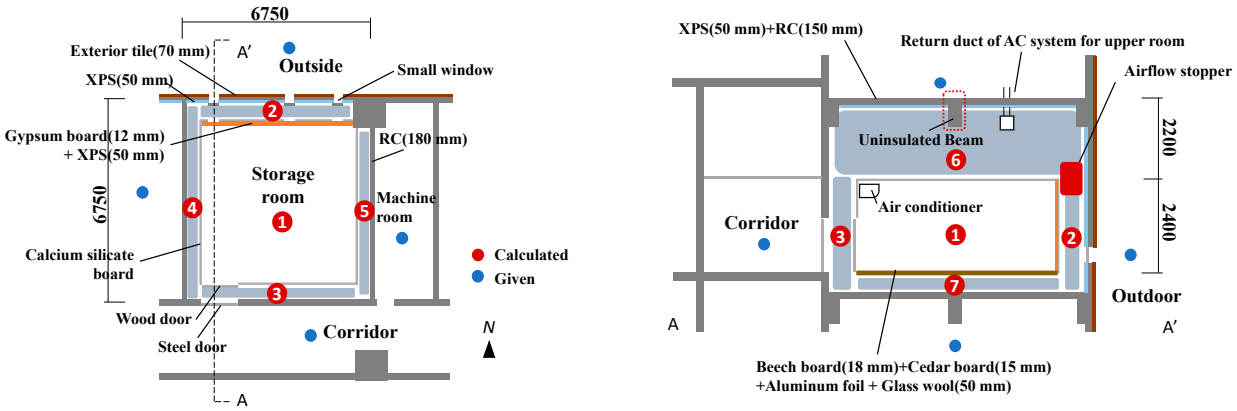

Figure 4. Outline of the storage room: (**a**) floor plan; (**b**) cross-sectional view A–A′.

Normally, no mechanical ventilation system was used in the room, and the three windows on the northern outer wall were usually closed. However, airflow through the gaps in the closed doors and windows could occur. Although an air conditioner was installed in the room, it was not normally used.

3.2. Numerical Model

The temperature and humidity in each space were assumed to be affected by the heat and moisture exchange with the material surface and the heat and moisture transport associated with the airflow between the spaces. The amount of airflow between each space was calculated using a multiroom airflow network model. The model accounted for the negative pressure in the south corridor of the storage room caused by the lavatory exhaust fan. The developed numerical model also considered the heat exchange with the air duct that passed through the attic space.

Because the north outer wall was exposed to direct solar radiation only for a brief period of time during the year, and the daily temperature fluctuation in the storage room was confirmed to be minimal throughout the year by measurements conducted in advance, the effect of solar radiation on the indoor temperature appeared to be small and had, therefore, been neglected in the numerical model. Museum staff worked only occasionally

and for a short duration in the room. Therefore, heat and moisture generation by the human body and the heat emission from lighting equipment were not considered.

3.3. Basic Equations

3.3.1. Air Heat and Moisture Balance in Each Space

The following heat and moisture balance equations were used to model the air in the storage room, four side buffer spaces, the attic space, and the crawl space (red circles in Figure 4a,b):

$$c_{air}\rho_{air}V_r\frac{\partial T_{a,r}}{\partial t} = \sum_{i=1}^{N_r}(h_r + h_c)S_i(T_{s,i} - T_{a,r}) + \sum_{j=1}^{M_r} c_{air}\left(G_{+j}T_{a,j} + G_{-j}T_{a,r}\right) + Q_{genr} \quad (1)$$

$$\rho_{air}V_r\frac{\partial X_{a,r}}{\partial t} = \sum_{i=1}^{N_r} h'S_i(p_{vs,i} - p_{va,r}) + \sum_{j=1}^{M_r}(G_{+j}X_{a,j} + G_{-j}X_{a,r}) + J_{genr} \quad (2)$$

where N_r is the number of walls in contact with space r, and M_r is the number of paths leading to space r. Subscript a represents the air in the space, and s represents the surface of the component. Subscripts r, i, and j indicate the space for which the heat and moisture balance is calculated, the wall that the space is in contact with, and the path leading to the space, respectively, and r = 1, 2, ... 7.

3.3.2. Heat and Moisture Transfer through Component Materials

The configurations of the wall, ceiling, floor, and air duct (hereinafter referred to as the components) are shown in Figure 4a,b. The heat and moisture balance equations of the components were as follows [29]:

$$(c\rho + c_w\rho_w\psi)\frac{\partial T}{\partial t} = \frac{\partial}{\partial x}\left[\lambda\frac{\partial T}{\partial x} + r\left\{\lambda'_{\mu g}\left(\frac{\partial \mu}{\partial x} - v_x g\right) + \lambda'_{Tg}\frac{\partial T}{\partial x}\right\}\right] \quad (3)$$

$$\rho_w\frac{\partial \psi}{\partial \mu}\frac{\partial \mu}{\partial t} = \frac{\partial}{\partial x}\left\{\lambda'_{\mu g}\left(\frac{\partial \mu}{\partial x} - v_x g\right) + \lambda'_{Tg}\frac{\partial T}{\partial x}\right\} \quad (4)$$

In the model, one-dimensional heat and moisture transfer in the direction of the component thickness was assumed. Because the moisture content in the wall material of the room was expected to remain in the hygroscopic region, only water vapor transfer was considered. The Robin boundary condition was applied to the surfaces of the building components, and the heat and moisture fluxes at the boundary were expressed as follows:

$$\left[-\lambda\frac{\partial T}{\partial x} - r\left\{\lambda'_{\mu g}\left(\frac{\partial \mu}{\partial x} - v_x g\right) + \lambda'_{Tg}\frac{\partial T}{\partial x}\right\}\right]_s = (h_r + h_c)(T_a - T_s) + rh'(p_{va} - p_{vs}) \quad (5)$$

$$\left[-\lambda'_{\mu g}\left(\frac{\partial \mu}{\partial x} - v_x g\right) - \lambda'_{Tg}\frac{\partial T}{\partial x}\right]_s = h'(p_{va} - p_{vs}) \quad (6)$$

Note that although the water chemical potential was used as the driving force for moisture transfer in Equation (3), the water vapor transfer on the component surfaces was described by the water vapor pressure, which was a function of the water chemical potential and temperature (the moisture transfer on the surface of the steel door, aluminum foil included in the inner floor, and exterior tiles were ignored).

3.3.3. Multizone Airflow Network Methods

A multizone airflow network consists of multiple spaces and airflow paths between them. The mass flow rate of air was calculated for the horizontal elements in the paths as follows:

$$G = \rho_{air}q(\Delta p)^{\frac{1}{n}} \quad (7)$$

and for the vertical elements as follows:

$$G = \frac{\rho_{air} q}{H_{TOP} - H_{BTM}} \int_{H_{BTM}}^{H_{TOP}} (\Delta p)^{\frac{1}{n}} dH \quad (8)$$

where the unit airflow rate, q, is the volume flow rate of air at a pressure difference of 1 Pa over the path. The static pressure at the floor level in each space and the mass flow rate of air through each path were determined simultaneously using the Newton–Raphson method so that the net mass flow rate of air entering each space was zero [30].

3.4. Calculation Parameters

3.4.1. Numerical Parameters of the Room

The thickness of the wooden support for the inner walls and ceilings was 100 mm or 45 mm, respectively (Figure 5). The area of each part is shown in Table 2. The materials and thicknesses of the other components are shown in Figure 4a,b.

The concrete slab of the floor above the attic space was divided into two parts, namely the part that was insulated and the part that was supported by the uninsulated beam. To be able to treat the heat transfer in the beam approximately as a one-dimensional problem, the equivalent area and thickness for the part supported by the beam were assumed such that they gave the same heat flux as that under two-dimensional heat flow and had the same volume as the original beam part. The thickness and area of the beam part were determined to be 47.6 cm and 14.37 m^2, respectively.

The values of the convective and radiative heat transfer coefficients, which were assumed to be the same for all the components, are shown in Table 3 [31–33]. The value of the convective heat transfer coefficient on the surface in contact with outdoor air was obtained by Jurges's Equation [31], assuming that the outside wind speed was 3 m/s. The value of the radiative heat transfer coefficient was determined considering the emissivity of the material surface [32]. The water vapor transfer coefficient was calculated from the convective heat transfer coefficient using the Lewis relationship [34]:

$$h' = \frac{h_c}{L_e c_{air} \rho_{air} R_v T_s} \quad (9)$$

The Lewis number was assumed to be 0.9 in the model.

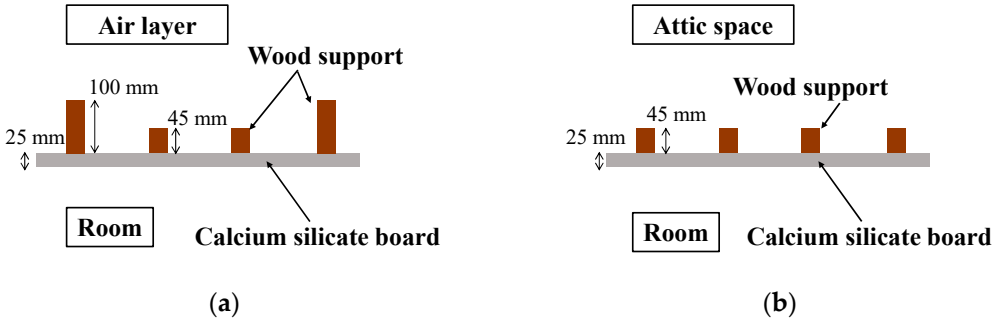

Figure 5. Structure of the inner wall and ceiling: (**a**) schematic horizontal section of the inner wall; (**b**) schematic vertical section of the ceiling.

Table 2. The area of the wall part without, with 100 mm, and with 45 mm thick wooden support (m^2).

	No Wooden Support	100 mm Wooden Support (mm)	45 mm Wooden Support (mm)
North wall	10.6	2.64	1.60
South wall	10.7	2.52	1.61
West wall	9.86	3.36	1.49
East wall	10.0	3.12	1.52
Ceiling	27.5	-	10.3

Table 3. Values of convective and radiative heat transfer coefficients.

		Surface in Contact with Indoor Space	Surface in Contact with Outdoor Air
h_c	(convective heat transfer coefficient; W/m^2·K)	4.10	18.0
h_r	(radiative heat transfer coefficient; W/m^2·K)	4.70	5.10

3.4.2. Material Properties

The hygrothermal material properties used in the calculation included the specific heat, thermal conductivity, moisture sorption isotherm, and vapor permeability. Figure 6 shows the moisture sorption isotherms of the calcium silicate board, wood, concrete, gypsum board, glass wool, and XPS used in the analysis. The quantity of water vapor adsorbed by the calcium silicate board was measured at various values of RH by using the gas-absorption method (Belsorp Max, Microtrac BEL Corp.). The results were used to determine the moisture sorption isotherm. The other hygrothermal properties and densities used in the study are listed in Table 4; they were taken from the literature [35–38]. The density and specific heat values were for the dry state. The vapor permeability for the water vapor pressure gradient was converted to $\lambda'_{\mu g}$ and λ'_{Tg} and used in the calculations. The values of thermal conductivity and vapor permeability were taken at 20 °C and in the range of 10−90% RH. For concrete, $\lambda'_{\mu g}$ and λ'_{Tg} were described as functions of the moisture content, where the value of $\lambda'_{\mu g}$ varied between 5.56×10^{-15} and 1.66×10^{-13}, and that of λ'_{Tg} between 5.25×10^{-11} and 1.40×10^{-9} at 20°C and 10–90% RH.

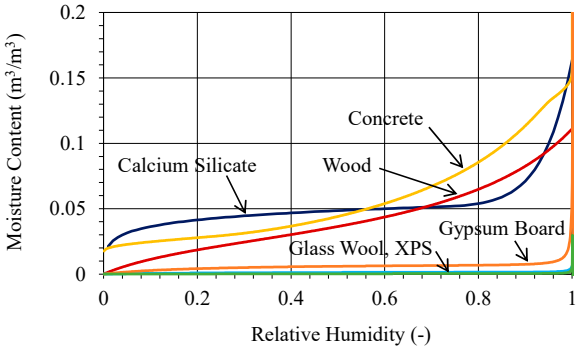

Figure 6. Moisture isotherms of materials.

Table 4. Hygrothermal properties and densities of materials.

	ρ	c (J/kg·K)	λ (W/m·K)	λ'_{pv}(kg/s·m·Pa)
Concrete	2303.2	1100	1.39~1.70	-
Gypsum boards	700	870	0.22	1.96×10^{-11} to 3.40×10^{-11}
Wood	365	1880	0.1	1.10×10^{-12}
Calcium silicate boards	946.8	760	0.16	7.33×10^{-12} to 2.89×10^{-11}
Glass wool	50	840	0.0325	1.58×10^{-10}
XPS	25	1470	0.0251	1.0×10^{-12}
Exterior tiles	2400	840	1.3	-
Steel	7870	442	80.3	-
Aluminum	2688	905	237	-

3.4.3. Conditions for a Multizone Airflow Network

The simulated multizone airflow network, comprising of eight spaces (the room, four side buffer spaces, attic space, crawl space, the corridor, and 16 paths), is shown in Figure 7. The gaps in the windows and doors were divided into vertical and horizontal elements (as

shown in Figure 8), and each was assigned a unit airflow rate. In this study, the air leakage characteristic value, n, discharge coefficient, α, and gap area, A, were used to determine the unit airflow rate, q, as follows:

$$\alpha A = q\left(\frac{\rho}{2}\right)^{\frac{1}{2}}(9.8)^{\frac{1}{n}-\frac{1}{2}} \quad (10)$$

Equation (10) is generally used for estimating the total equivalent gap area [39].

The air leakage characteristic value, n, and the unit airflow rate, q, used in the calculations are shown in Table 5. Although these parameters are normally identified experimentally, it was difficult to measure them in the storage room. Therefore, the air leakage characteristic value and gap area were estimated from the shape of the gap, and the discharge coefficient, α, was assumed as 0.6.

On path 15 (three windows between the north buffer space and outdoor air in Figure 7a,b), the wind pressure, calculated from the wind direction and wind speed averaged over 10 min, was added to the pressure difference.

To consider the negative pressure in the corridor due to the operation of the lavatory fan (described earlier), a constant value was added to the pressure difference on path 16 (Figure 7b) that discharged the air from the corridor to the outdoor air. Several combinations of unit airflow rate and pressure difference were preliminarily studied, and the calculated results were compared to the measured humidity ratios and temperatures in the room and the northern buffer space. Among these combinations, the calculated values of the temperature and humidity ratio at a unit airflow rate of 1.28 $m^3/s{\cdot}Pa^{1/2}$ and additional pressure of 7.5 Pa were in good agreement with the measured values.

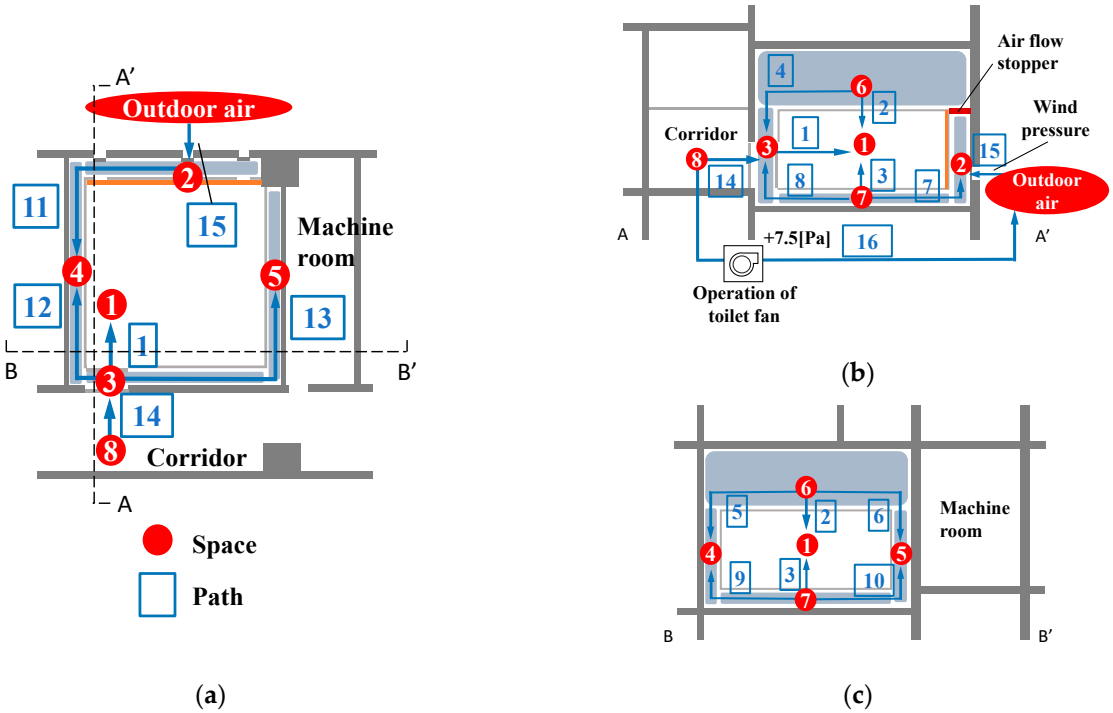

Figure 7. Ventilation network of the storage room: (**a**) horizontal section; (**b**) cross section A–A′; (**c**) cross section B–B′.

3.4.4. Heat Flow from Air Duct

For the heat flow from the duct, UA_{duct} ($T_{Upper\ Floor} - T_{Attic\ space}$; W) was added to the heat balance of the attic space, assuming the heat transmission coefficient, U, as 1.25 $W/m^2{\cdot}K$ and the duct area, A_{duct}, as 5.26 m^2 ($T_{Upper\ Floor}$ and $T_{Attic\ space}$ indicate the temperature of the upper floor and that of the attic space, respectively). The condensation on the surface of the duct would likely occur, leading to a degradation in the insulation

performance of glass wool. In this numerical model, the thermal conductivity of wet glass wool was assumed to be 0.07 W/m·K, which was twice as high as in dry conditions.

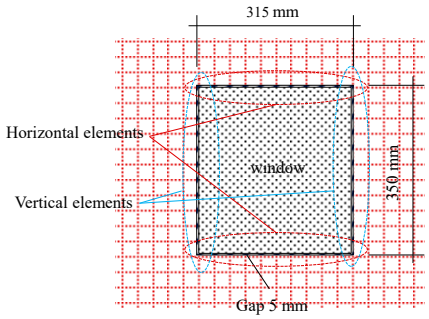

Figure 8. Schematic of the window gap.

Table 5. Airflow paths and their flow characteristics.

Path	Assigned Gaps	n (-)	Horizontal q ($m^3/s \cdot Pa^{1/n}$)	Vertical q ($m^3/s \cdot Pa^{1/n}$)
1	Gap in the inner door	1.5	0.00327	0.0118
2	Gaps in the inspection window of ceiling and light fixtures	1.5	0.0251	-
3	Gap between the floor and wall	1.5	0.0129	-
4	Gap between the attic space and south buffer space	2.0	0.826	-
5, 6	Gaps between the attic space and east/west buffer space	2.0	0.819	-
7, 8	Gaps between the crawl space and north/south buffer space	2.0	0.552	-
9, 10	Gaps between the crawl space and east/west buffer space	2.0	0.548	-
11, 12, 13	Gaps between the north and west buffer space and the gaps between the south and west/east buffer space	2.0	-	0.321
14	Gap in the corridor side door	1.5	0.00327	0.00591
15	Gaps in the windows between the outdoor air and north buffer space	1.5	0.00082	0.000915

3.4.5. Conditions of Surrounding Areas

The temperature and RH of the east and west rooms of the subject storage room, corridor, outdoor air, and upper- and lower-floor rooms (the blue circles in Figure 4a,b) were input-based on the measured data and updated at each time step of the analysis. The values of temperature and RH were assumed to change linearly during the measurement interval. The temperatures and RHs in the storage room, the attic space, the northern buffer space, the south corridor, the adjoining rooms to the east and west, and the room directly above were also measured [4]. The measurements started in February 2018, except for the room on the upper floor, whose data were not available until early October 2018. Figure 9 shows the temperatures and RHs in the upper and lower floors of the storage room used in the calculations. For the upper-floor room, the setpoint of the AC system (21 °C, 49% RH) was assumed as the input data before the measurements started. The AC system was unintentionally stopped and restarted on 21 December 2018. Furthermore, the humidifier of the AC system was out of order for approximately two months after the AC system restart, and thus the RH was lower.

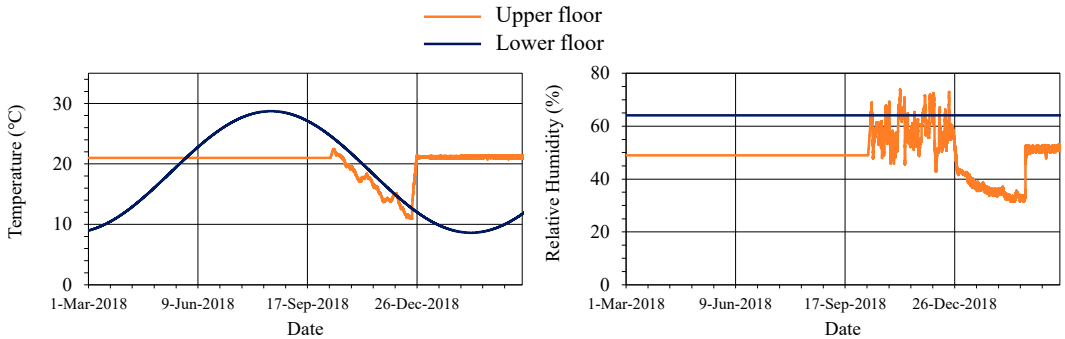

Figure 9. Input temperatures and RHs for the upper and lower rooms.

Because no measurements were carried out for the room directly under the storage room, the temperature was assumed to fluctuate over one year, following a cosine pattern, whose amplitude was determined based on the measured temperatures in the other room on the underfloor. The RH was assumed as a constant value equal to the annual average for the room. The outdoor air temperature, RH, wind direction, and wind speed were based on meteorological data for Kyoto city obtained from the Japan Meteorological Agency's website [40].

3.4.6. Numerical Calculation Settings

The basic equations were discretized with a central difference scheme in the space, and the element size of each material was as follows: 2 mm for wood, calcium silicate boards, gypsum boards, and glass wool; 5 mm for XPS; 10 mm for concrete and exterior tiles; and 25 mm for steel. The explicit method was used to solve the equations, and the time step was set to 1 s. The calculation program was written using Fortran 90, and the solution was confirmed to be not divergent. It took approximately 15 h to calculate one year in the simulation.

The numerical analysis was performed for a year starting from 1 March 2018. For the initial conditions, measured data were used for the storage room, the attic space and the northern buffer space. The temperatures and RHs of the south, east, and west buffer space, and the crawl space were set to be the same as in the storage room. The water chemical potentials and temperatures on the material surfaces were assumed to be in equilibrium with the air in contact with the surface, and their values across the thickness of all materials were assumed to vary linearly.

3.4.7. Evaluation of Possible Factors Causing High Humidity in the Storage Room

As explained earlier, the negative pressure in the corridor caused by the operation of the lavatory fan and the indirect cooling by the AC system of the upper-floor room were potential factors causing the high humidity in the storage room. We could quantitatively evaluate the impact of a factor on the humidity in the room by comparing the temperature and humidity under the current conditions and under conditions in which the factor variation was suppressed.

The authors conducted the analysis for CASES 0–4 listed in Table 6 and compared the calculated temperature and humidity in the storage room for CASES 1–4 to the baseline CASE 0, focusing on the summer months (June–September). In CASE 1, the operation of the lavatory fan was stopped to prevent moisture gain associated with the inflow of humid outdoor air, and, thus, there was no additional pressure in path 16. In CASE 2, assuming that the windows facing the outdoor air were made airtight, the unit airflow rate through the gaps in the windows was reduced to 10%. In CASE 3, to reduce the indirect cooling by the AC system, the duct insulation (glass wool) was modified by changing its thermal conductivity value to that in dry conditions. In CASE 4, a 50 mm layer of XPS was attached to the uninsulated RC beam to improve the thermal insulation. The thickness of XPS for one-dimensional calculations was estimated to be 23.2 mm from the preliminary two-dimensional heat transfer simulation.

Table 6. Conditions of each CASE.

CASE	Modification	Parameter Change
0	Baseline conditions	No change
1	Stopping of lavatory fans	Reducing added pressure on path 16 7.5→0 (Pa)
2	Air-tightening of the window gaps	Reducing the unit airflow rate of path 15 (window gaps) to 10%
3	Modification of the duct insulation	Reducing the thermal conductivity of glass wool around duct 0.07→0.035 (W/m·K)
4	Insulating the building beam	Attaching of 50 mm of XPS to the beam of the building frame

4. Results

4.1. Verification of the Proposed Model

The validity of the numerical model was confirmed by comparing the measured and simulated values of room temperature, RH, and humidity ratio for one year starting 1 March 2018. While verifying the model outputs, the operation of the air conditioner was considered, and the constant heat it generated was included in the heat balance in the storage room during its operation. The amounts of the heat generated were estimated by comparing the calculated and measured temperatures of the room as −450 W (1 August 2:00 p.m. to 9 August 3:00 p.m.) and −150 W (20 August 1:00 p.m. to 27 August 1:00 p.m.).

The calculated and measured temperatures, humidity ratios, and RHs in the storage room are shown in Figure 10. The measured humidity ratio is the value converted from the measured temperature and RH. The annual mean absolute errors between the calculated and measured values of temperature, humidity ratio, and RH were 0.36 °C, 0.00041 kg/kg', and 2.7% RH, respectively, and, thus, we concluded that the numerical model reasonably simulated the measured values. The calculated RH exceeded 45% during the year and reached 70% in the summer months, similar to the measured results.

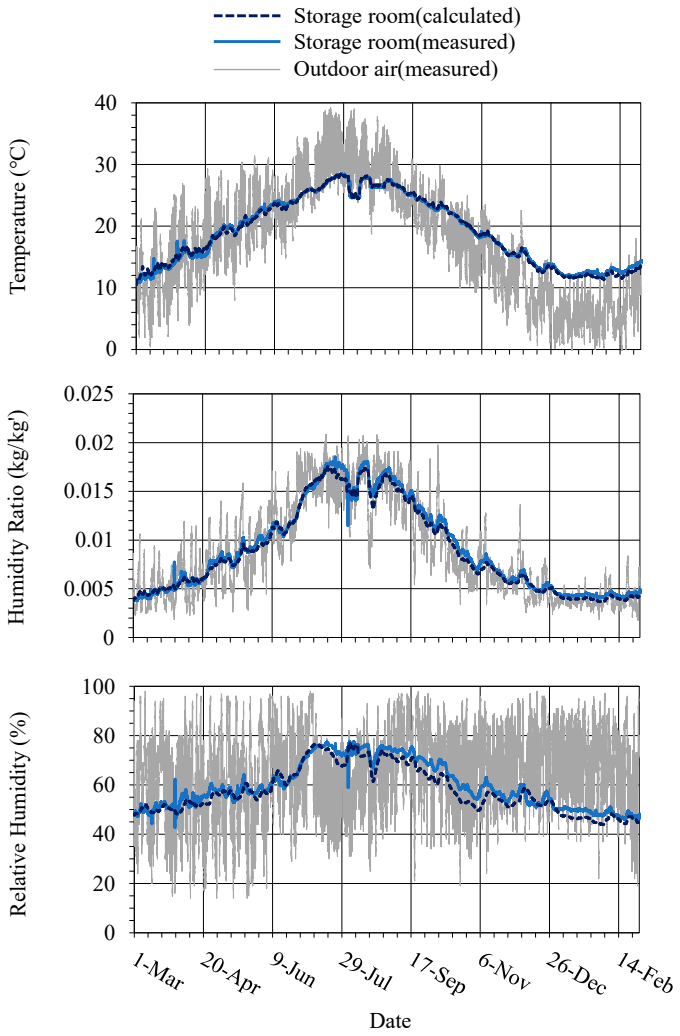

Figure 10. Calculated and measured temperatures, humidity ratios, and RHs in the storage room.

4.2. Effect of Each Factor (Numerical Results)

4.2.1. Temperature and Humidity in the Storage Room

The temperatures, humidity ratios, and RHs in the room in CASES 0–4 are shown in Figure 11. In CASES 1 and 0, the variation in temperature was similar (an average

increase of 0.058 °C), and the variation in the humidity ratio and the RH was suppressed. In CASE 1, the humidity ratio was reduced by an average of 0.0010 kg/kg', and the RH by an average of 4.6% RH; these results differed from those of CASE 0. In CASE 2, the temperature variation was similar to that of CASE 0, and the humidity ratio decreased by 0.00091 kg/kg'. The average RH decreased by 3.9% RH compared to that of CASE 0. In CASE 3, the temperature increased slightly (an average of 0.028 °C), and the humidity ratio varied similarly to that in CASE 0. Consequently, the RH varied in a similar way to that of CASE 0 (an average decrease of 0.11% RH). In CASE 4, the temperature increased by 0.17 °C, and the humidity ratio and the RH varied similarly to that in CASE 0 (an average decrease of 0.64% RH).

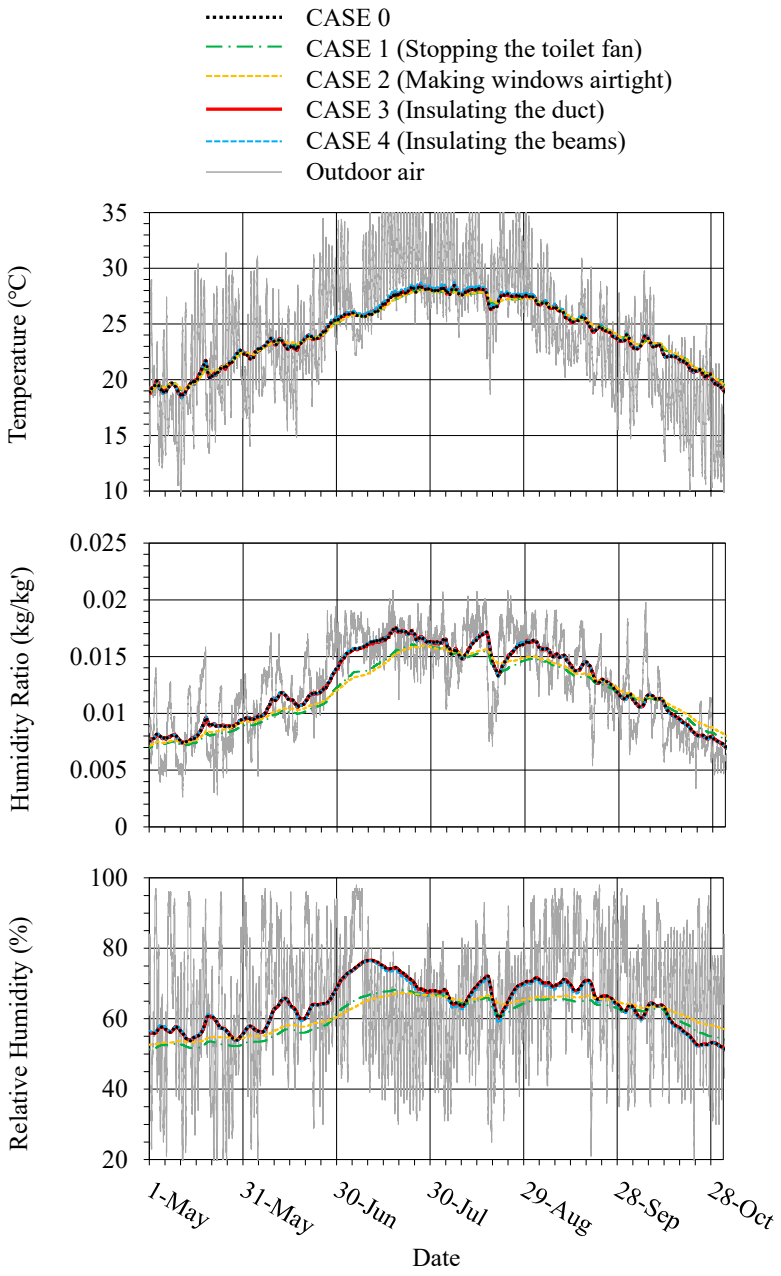

Figure 11. Temperature, humidity ratio, and RH in the storage room in each CASE.

4.2.2. Heat and Moisture Transfer into and out of the Storage Room

Figure 12 shows the daily average of moisture flow into the room in CASES 0, 1, and 2. In CASE 0, the moisture flow into the storage room fluctuated wildly, with daily average

values ranging from +9.34 × 10^{-7} to −1.92 × 10^{-6} kg/s. In both CASES 1 and 2, the fluctuations of the moisture flow into the room were smaller than that in CASE 0. In CASE 1, the range of amplitude of the daily average of moisture inflow was from −1.06 × 10^{-6} to 5.66 × 10^{-7}, while in CASE 2 it was from −5.57 × 10^{-7} to 3.39 × 10^{-7}.

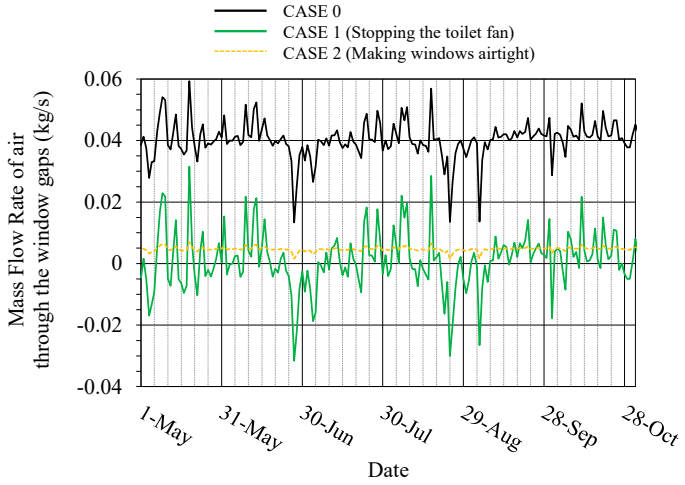

Figure 12. Daily averages of moisture inflow to the storage room in CASES 0, 1, and 2.

The daily average mass flow rates of air through the window gaps (path 15) in CASES 0, 1, and 2 are shown in Figure 13. Positive values indicated the inflow of outdoor air into the north side buffer space, while negative values indicated the outflow. There was a constant inflow of outdoor air of about 0.0133 to 0.0569 kg/s in CASE 0, and the average value from June to September was 0.0396 kg/s. In CASE 1, the flow rate of air fluctuated between −0.0315 and +0.028 kg/s with alternating inflows and outflows, and the average flow rate was 0.00064 kg/s. In CASE 2, there was a constant inflow of about 0.005 kg/s. The fluctuations were slight, and the average was 0.0047 kg/s.

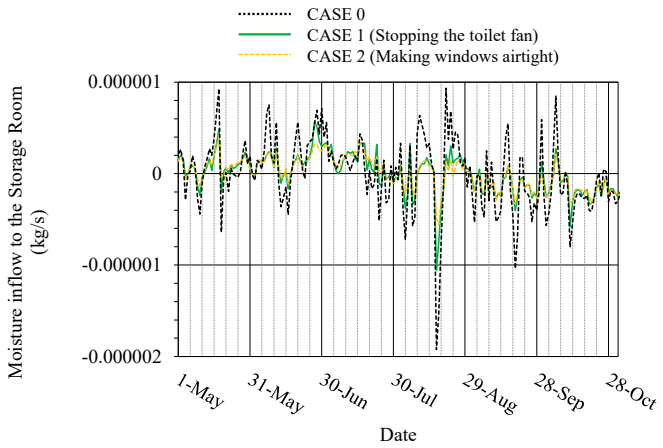

Figure 13. Mass flow rates of air through the window gaps (path 15) in CASES 0, 1, and 2.

The daily average values of the total heat inflow to the storage room in CASES 3 and 4 are shown in Figure 14a,b, respectively. In CASE 3, the heat loss from the room through the ceiling was reduced by approximately 2.0 W compared to CASE 0. However, the heat flow through the other components decreased, and the total heat acquisition hardly increased (by 7.28 × 10^{-5} W on average). In CASE 4, the heat loss through the ceiling decreased by about 8.0 W compared to CASE 0, but the total heat acquisition did not increase (an average increase of 6.78 × 10^{-4} W).

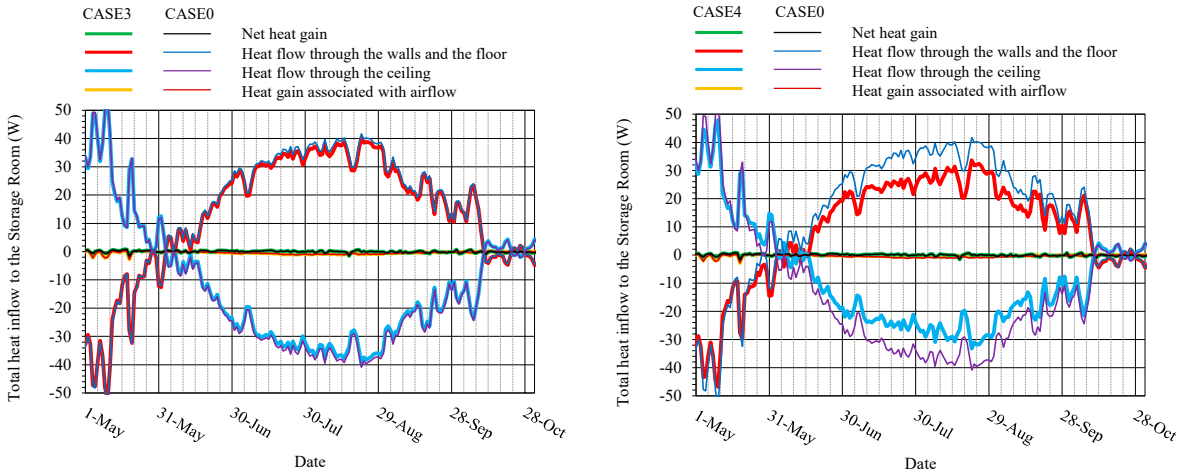

(**a**) (**b**)

Figure 14. Comparison of the heat flow into the storage room: (**a**) total heat inflow to the storage room in CASES 0 and 3; (**b**) total heat inflow to the storage room in CASES 0 and 4.

Figure 15a,b show the total heat inflow to the attic space in CASES 3 and 4, respectively. In CASE 3, the heat flow to the duct was reduced during the summer months, and the heat loss was reduced from 3.18×10^8 J to 1.87×10^8 J when integrated during the summer months (from June to September), being 58.8% of the heat loss of CASE 0. Similarly, in CASE 4, the heat flow to the beam was reduced compared to that in CASE 0, while the heat loss from the attic space was reduced from 1.24×10^9 J to 4.94×10^8 J, being 39.9% of that in CASE 0.

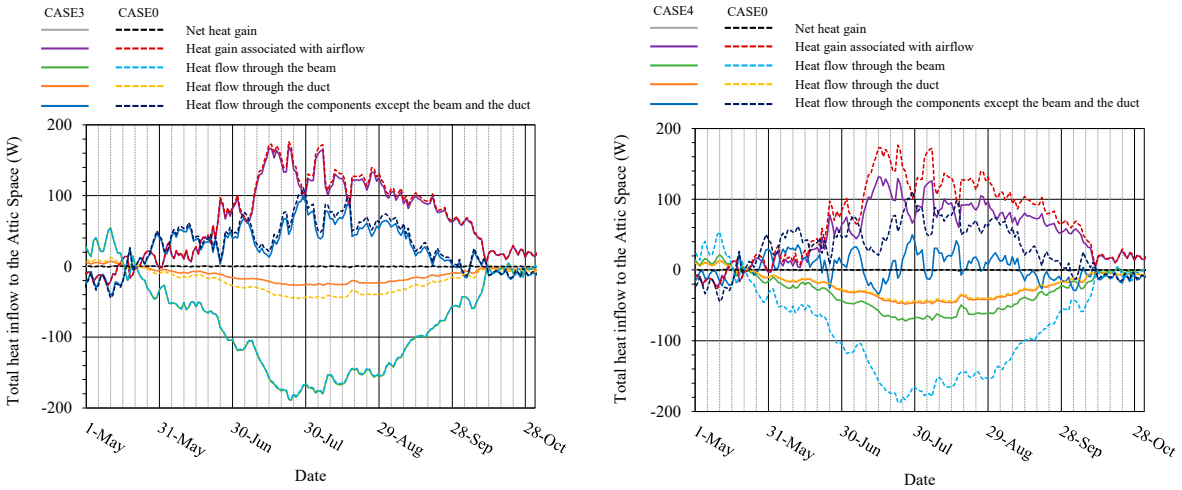

(**a**) (**b**)

Figure 15. Comparison of the heat flow into the attic space: (**a**) total heat inflow to the attic space in CASES 0 and 3; (**b**) total heat inflow to the attic space in CASES 0 and 4.

5. Discussion

In CASE 1, when the lavatory fan was stopped, the high humidity ratio in the room during the summer was suppressed, and the RH in the room was reduced. Similarly, in CASE 2, when the airtightness of the windows was improved, the high RH in the room was suppressed. The amount of the outdoor air flowing into the northern buffer space was reduced in CASES 1 and 2 compared to CASE 0. Although an airflow stopper (glass

wool wrapped in plastic sheet) was placed between the northern buffer space and the attic space, the air could still move between the surrounding spaces along paths 4–13. The air in the surrounding spaces could enter the storage room through the gaps in the inner walls (paths 1–3). By stopping the fan or improving the airtightness of the windows, the buffer space on the north side and other spaces around the storage room became less affected by the outdoor air, and the moisture balance in the room was less influenced by the moisture from the outdoor air. Note that The RH and humidity ratio in the room in CASES 1 and 2 were higher than CASE 0 after 28 September because the moisture buffering effect of the building components maintained the humidity in the room even after the humidity ratio of the outdoor air became low. Among the possible factors, the inflow of humid outdoor air through the window gaps, accelerated by the negative pressure on the corridor side caused by operating the lavatory fan, affected the high humidity in the storage room during summer. The airtightness of the building that houses the storage space affected the dehumidification load, and this result agreed with those available in the literature [14,23]. For the storage room with a structure with buffer spaces, outdoor air flew into the buffer space, and the air in the buffer space flew into the room through gaps in the inner building components, causing the moisture balance in the room to be affected by humidity fluctuations in the outdoor air. Notably, the hygrothermal environment for the artifact conservation was deteriorated, not only by the improper hygrothermal building performance of the storage room but also by the ventilation system of the surrounding rooms, because the operation of the lavatory fan accelerated the inflow of outdoor air into the subject room.

In CASE 3, when the duct insulation was modified, and in CASE 4, when the beam was insulated, the temperature in the storage room increased slightly, but the RH hardly decreased. It was confirmed by additional simulations that the increased thickness of glass wool around the duct and XPS attached to the beam did not have a significant effect on suppressing the high RH in the room. In the heat balance of the attic space, the heat flow from the adjacent space, including the heat flow from the storage room, was suppressed by insulating the duct or the beam. The total heat gain of the storage room did not increase because of the significant effect of the heat flow through the walls and the floor. In another simulation, the heat gain associated with the airflow, which had a large effect on the heat balance in the attic space, was also suppressed by stopping the lavatory fan, and it was confirmed that the increase in the net heat gain in the room was not significant compared to that in CASE 1. However, the suppression of heat loss through the duct in CASE 3 and to the beam in CASE 4 would lead to reducing the energy loss of the AC system for the upper floor. In addition, the insulation of the beam could reduce the risk of condensation.

6. Conclusions

In order to control the hygrothermal environment of the storage room with buffer spaces used for metal cultural artifacts storage and ensure low humidity for their conservation, this study developed a numerical model of the storage room hygrothermal environment and evaluated potential factors contributing to the high humidity measured in the storage room.

The numerical model was developed by adopting a formulation of the simultaneous heat and moisture transfer within the building materials and ventilation network to calculate the heat and moisture balance considering the heat and moisture capacities of the building and the airflow through the gaps in the building components. The calculated temperature, humidity ratio, and RH in the room were compared to the measured values for one year, and the validity of the numerical model was confirmed.

The factors that produced the high humidity in the storage room during the summer months, i.e., the inflow of the outdoor air and indirect cooling by an AC system on the upper floor, were evaluated using the proposed numerical model. When the lavatory fan was stopped or the windows were made airtight, the high humidity in the storage room was suppressed below 70% RH. The high humidity in the storage room during summer

was caused by the inflow of humid outdoor air through the gaps in the windows, which was accelerated by the lavatory fan. In the storage room with a structure surrounded by buffer spaces, the humid outdoor air entering into the buffer spaces affected the moisture balance in the room by airflow through the gaps in the inner components. In contrast, the increase in temperature and decrease in RH in the room were small when the thermal insulation around the duct and the building frame beam improved. The improvement to the insulation suppressed the heat loss to the AC system, but the amount of heat gain in the room was not largely changed. The indirect cooling by the AC system through the duct or the beam had little effect on the high RH in the room. However, the heat loss to the duct or the beam would be significant for the energy loss of the AC system and the risk of damage to the building due to condensation.

In future research, we will use the numerical model developed in this study to propose a method for achieving low humidity in the storage room suitable for the conservation of metal cultural artifacts. We will investigate the potential of controlling the inflow of outside air by improving the airtightness of the windows and changing the operational method of the ventilation system as well as methods of environmental control using AC systems such as dehumidifiers.

Author Contributions: Conceptualization, K.I., C.I., and S.H.; methodology, K.I., C.I., and D.O.; validation, K.I., C.I., and D.O.; investigation, K.I., C.I., and M.Y.; data curation, K.I.; writing—original draft preparation, K.I.; writing—review and editing, C.I., D.O., and S.H.; supervision, S.H. and M.Y.; funding acquisition, C.I., D.O., and S.H. All authors have read and agreed to the published version of the manuscript.

Funding: This research was funded by the Jyukankyo Foundation 2020.

Institutional Review Board Statement: Not applicable.

Informed Consent Statement: Not applicable.

Data Availability Statement: Not applicable.

Conflicts of Interest: The authors declare no conflict of interest.

Nomenclature

Symbol	Unit	Meaning
A	m^2	Area of opening or gap
c	J/kg·K	Specific heat of material
c_{air}	J/kg·K	Specific heat of air
c_w	J/kg·K	Specific heat of liquid water
g	kg·m/s^2	Gravitational acceleration
G	kg/s	Mass flow rate of air
G_{+j}	kg/s	Mass flow rate of air through path j into each space
G_{-j}	kg/s	Mass flow rate of air through path j out of each space
h_r	W/m^2·K	Radiative heat transfer coefficient
h_c	W/m^2·K	Convective heat transfer coefficient
h'	kg/s·m^2·Pa	Moisture transfer coefficient
H_{TOP}	m	Height of top of opening
H_{BTM}	m	Height of bottom of opening
J_{gen}	kg/s	Moisture generation in space
L_e	-	Lewis number
n	-	Air leakage characteristic value
p_v	Pa	Water vapor pressure
Δp	Pa	Pressure difference between adjacent spaces
q	m^3/s·Pa$^{1/n}$	Unit airflow rate
Q_{gen}	W	Heat generation in space
r	J/kg	Latent heat of water evaporation
R_v	Pa·m^3/kg·K	Specific gas constant of water vapor

S	m^2	Area of component
t	s	Time
T	K	Temperature
$T_{a,j}$	K	Temperature on the other side of path j
v_x	-	x-direction component of the vertically downward unit vector v
V	m^3	Volume of space
X	kg/kg′	Humidity ratio
$X_{a,j}$	kg/kg′	humidity ratio on the other side of path j
α	-	Discharge coefficient
λ	W/m·K	Thermal conductivity
λ'_{p_v}	kg/s.m.Pa	Water vapor permeability
λ'_{Tg}	kg/s.m.K	Moisture conductivity by temperature difference
$\lambda'_{\mu g}$	kg/s.m.(J/kg)	Moisture conductivity by water chemical potential difference
μ	J/kg	Chemical potential of free water
ρ	kg/m^3	Density of material
ρ_w	kg/m^3	Density of liquid water
ρ_{air}	kg/m^3	Density of air
ψ	m^3/m^3	Moisture content of material element

References

1. Thomson, G. *The Museum Environment*, 2nd ed.; Butterworth-Heinemann: Oxford, UK, 1986.
2. Erhardt, D.; Mecklenburg, M. Relative humidity re-examined. In Proceedings of the Preventive Conservation Practice, Theory and Research, Ottawa, ON, Canada, 12–16 September 1994.
3. Harriman, L.G.; Brundrett, G.W.; Kittler, R. *Humidity Control Design Guide for Commercial and Institutional Buildings*; American Society of Heating, Refrigerating and Air Conditioning Engineers, Inc.: Atlanta, USA, 2001.
4. Ishikawa, K.; Iba, C.; Ogura, D.; Hokoi, S.; Yokoyama, M. Commissioning of air- conditioning and ventilation systems in a public museum storing historical cultural properties. In Proceedings of the REHABEND 2020, Granada, Spain, 24–27 March 2020.
5. Ferdyn-Grygierek, J.; Kaczmarczyk, J.; Blaszczok, M.; Lubina, P.; Koper, P.; Bulińska, A. Hygrothermal Risk in Museum Buildings Located in Moderate Climate. *Energies* **2020**, *13*, 344. [CrossRef]
6. Grunewald, J.; Ruisinger, U.; Häupl, P. The Rijksmuseum Amsterdam-Hygrothermal Analysis and Dimensioning of Thermal insulation. In Proceedings of the 3rd International Building Physics Conference, Montreal, QC, Canada, 27–31 August 2006; pp. 345–352.
7. Agency for Cultural Affairs of Japan. Guidelines for the Planning of Facilities Exhibiting Cultural Property. 1995. Available online: https://www.bunka.go.jp/seisaku/bunkazai/hokoku/shisetsu_shishin.html (accessed on 9 May 2021). (In Japanese)
8. Ferdyn-Grygierek, J. Monitoring of indoor air parameters in large museum exhibition halls with and without air-conditioning systems. *Build. Environ.* **2016**, *107*, 113–126. [CrossRef]
9. Kramer, R.P.; Schellen, H.L.; van Schijndel, A.W.M. Impact of ASHRAE's museum climate classes on energy consumption and indoor climate fluctuations: Full-scale measurements in museum Hermitage Amsterdam. *Energy Build.* **2016**, *130*, 286–294. [CrossRef]
10. Grabon, M.; Anderson, J.; Bushnell, P.; Calvo, A.; Chadwick, W. The Sistine Chapel: New HVAC System for Cultural Preservation. *ASHRAE J.* **2015**, *57*, 20–34.
11. Cadelano, G.; Cicolin, F.; Emmi, G.; Mezzasalma, G.; Poletto, D.; Galgaro, A.; Bernardi, A. Improving the Energy Efficiency, Limiting Costs and Reducing CO2 Emissions of a Museum Using Geothermal Energy and Energy Management Policies. *Energies* **2019**, *12*, 3192. [CrossRef]
12. Kompatscher, K.; Kramer, R.; Ankersmit, B.; Schellen, H. Intermittent conditioning of library archives: Microclimate analysis and energy impact. *Build. Environ.* **2019**, *147*, 50–66. [CrossRef]
13. Schito, E. Application of different methodologies for artwork risk assessment and reduction: Simulation of a museum room with a validated dynamic model. *IOP Conf. Ser. Mater. Sci. Eng.* **2020**, *949*, 012001. [CrossRef]
14. Janssen, H.; Christensen, J.E. Hygrothermal optimisation of museum storage spaces. *Energy Build.* **2013**, *56*, 169–178. [CrossRef]
15. Jørgen, E. Hygrothermal evaluation of a museum storage building based on actual measurements and simulations. *Energy Procedia* **2015**, *78*, 651–656.
16. Neuhaus, E.; Schellen, H.L. Conservation heating for a museum environment in a monumental building. In Proceedings of the 10th Conference on the Thermal Performance of the Exterior Envelopes of Whole Buildings, Clearwater Beach, FL, USA, 2–7 December 2007.
17. Larsen, P.K. Heat pumps for conservation heating in churches. In Proceedings of the Third International Conference on Energy Efficiency in Historic Buildings, Visby, Sweden, 26–27 September 2018; pp. 311–317.

18. Ferdyn-Grygierek, J.; Grygierek, K. HVAC control methods for drastically improved hygrothermal museum microclimates in warm season. *Build. Environ.* **2019**, *149*, 90–99. [CrossRef]
19. Ferdyn-Grygierek, J.; Grygierek, K. Proposed Strategies for Improving Poor Hygrothermal Conditions in Museum Exhibition Rooms and Their Impact on Energy Demand. *Energies* **2019**, *12*, 620. [CrossRef]
20. Larsen, P.K.; Broström, T. Climate control in historic buildings in Denmark. In Proceedings of the World Renewable Energy Congress 2011 (WREC 2011), Linkoping, Sweden, 8–13 May 2011.
21. Ryhl-Svendsen, M.; Jensen, L.A.; Larsen, P.K.; Padfield, T. Does a Standard Temperature Need to Be Constant? Presented at the Going Green; towards Sustainability in Conservation. The British Museum, London, UK, 24 April 2009. Available online: http://www.conservationphysics.org/standards/standardtemperature.php (accessed on 9 May 2021).
22. Napp, M.; Kalamees, T. Energy use and indoor climate of conservation heating, dehumidification and adaptive ventilation for the climate control of a mediaeval church in a cold climate. *Energy Build.* **2015**, *108*, 61–71. [CrossRef]
23. Padfield, T.; Ryhl-Svendsen, M.; Larsen, P.K.; Jansen, L.A. A review of the physics and the building science which underpins methods of low energy storage of museum and archive collections. *Stud. Conserv.* **2018**, *63*, 209–215. [CrossRef]
24. Padfield, T.; Larsen, P.K.; Jensen, L.A.; Ryhl-Svendsen, M. The potential and limits for passive air conditioning of museums, stores and archives. In Proceedings of the Museum Microclimates, Copenhagen, Denmark, 19–23 November 2007.
25. Ryhl-Svendsen, M.; Padfield, T.; Smith, V.A.; Santis, F.D. The indoor climate in historic buildings without mechanical ventilation systems. In Proceedings of the Healthy Buildings 2003-7th International Conference, National University of Singapore, Singapore, 7–11 December 2003; Volume 2, pp. 278–283.
26. Sciurpi, F.; Carletti, C.; Pierangioli, L. Assessment of thermo-hygrometric indicators for preventive conservation inside museums: In field monitoring and passive microclimatic control strategies applied to "La Specola" museum of Florence. *IOP Conf. Ser. Mater. Sci. Eng.* **2018**, *364*, 012023. [CrossRef]
27. de Guichen, G. Climate in Museums. ICCROM. 1988. Available online: https://www.iccrom.org/publication/climate-museums-measurement-climat-dans-le-musee-mesure (accessed on 9 May 2021).
28. Onset Company's Website. Available online: https://www.onsetcomp.com/products/data-loggers/ux100-011a/ (accessed on 31 May 2021).
29. Matsumoto, M.; Iwamae, A. An analysis of temperature and moisture variations in the ground under natural climatic conditions. *Energy Build.* **1988**, *11*, 221–237. [CrossRef]
30. Matsushita, T. Study on Prediction of Smoke Movement for Evaluation of Evacuation Safety in Case of a Fire. Ph.D. Thesis, Kyoto University, Kyoto, Japan, 1994. (In Japanese)
31. Jürges, W. Der Wärmeübergang an eiener ebenen Wand. *Beih. Z. Gesundh. Ing.* **1924**, *19-1*, 51.
32. Szokolay, S.V. *Introduction to Architectural Science the Basis of Sustainable Design*, 3rd ed.; Routledge: Oxfordshire, UK, 2014.
33. Wilkes, C.B.; Petersen, C.M.F. Radiation and convection from surfaces in various positions. *ASHVE Trans.* **1938**, *44*, 513.
34. Eckert, E.R.; Drake, R.M., Jr. *Analysis of Heat and Mass Transfer*; McGraw Hill: New York, NY, USA, 1972; p. 733.
35. Kumaran, M.K. Final Report Volume 3 Task 3: Materal Properties. In *Energy Conservation in Buildings and Community Systems*; International Energy Agency: Paris, France, 1996.
36. AIJES-H001-2006. *Academic Standards for Measurement of Moisture Properties*; Architectural Institute of Japan: Tokyo, Japan, 2006. (In Japanese)
37. Japan Society of Thermophysical Properties. *Thermophysical Properties Handbook*; Yokendo Ltd.: Tokyo, Japan, 1990. (In Japanese)
38. Ogura, D. Study on Heat and Moisture Behavior in Underground Space. Ph.D. Thesis, Kobe University, Hyogo, Japan, 2000. (In Japanese)
39. JIS A 2201. *Test Method for Performance of Building Airtightness by Fan Pressurization*; Japanese Industrial Standards: Tokyo, Japan, 2017. (In Japanese)
40. Japan Meteorological Agency's Website. Available online: http://www.jma.go.jp/jma/menu/menureport.html (accessed on 9 May 2021).